

Can Specific THz Fields Induce Collective Base-Flipping in DNA?  
A Stochastic Averaging and Resonant  
Enhancement Investigation  
Based on a New Mesoscopic Model

Wang Sang Koon\*, Houman Owhadi†, Molei Tao‡, Tomohiro Yanao§

March 15, 2024

**Abstract**

We study the metastability, internal frequencies, activation mechanism, energy transfer, and the collective base-flipping in a mesoscopic DNA via resonance with specific electric fields. Our new mesoscopic DNA model takes into account not only the issues of helicity and the coupling of an electric field with the base dipole moments, but also includes environmental effects such as fluid viscosity and thermal noise. And all the parameter values are chosen to best represent the typical values for the opening and closing dynamics of a DNA. Our study shows that while the mesoscopic DNA is metastable and robust to environmental effects, it is vulnerable to certain frequencies that could be targeted by specific THz fields for triggering its collective base-flipping dynamics and causing large amplitude separation of base pairs. Based on applying Freidlin-Wentzell method of stochastic averaging and the newly developed theory of resonant enhancement to our mesoscopic DNA model, our semi-analytic estimates show that the required fields should be THz fields with frequencies around 0.28 THz and with amplitudes in the order of 450 kV/cm. These estimates compare well with the experimental data of Titova et al., which have demonstrated that they could affect the function of DNA in human skin tissues by THz pulses with frequencies around 0.5 THz and with a peak electric field at 220 kV/cm. Moreover, our estimates also conform to a number of other experimental results which appeared in the last couple years.

---

\*Corresponding Author. koon@caltech.edu. Control and Dynamical Systems, California Institute of Technology, Pasadena, California, 91125

†owhadi@caltech.edu. Applied and Computational Mathematics and Control and Dynamical Systems, California Institute of Technology, Pasadena, California, 91125

‡mtao@gatech.edu. School of Mathematics, Georgia Institute of Technology, Atlanta, Georgia, 30332

§yanao@waseda.jp. Department of Applied Mechanics and Aerospace Engineering, Waseda University, Tokyo, Japan

Our study shows that while the mesoscopic DNA is metastable and robust to environmental effects, it is vulnerable to certain frequencies that could be targeted by specific THz fields for triggering its collective base-flipping dynamics and causing large amplitude separation of base pairs. Though more work may still be needed to take into consideration the issue of modeling the pulses, we believe that, even as it stands right now, our new mesoscopic DNA model and semi-analytical estimates have suggested resonance as a possible mechanism for the experimental results mentioned above, and hopefully will inspire new experimental designs that may settle this question. Furthermore, our semi-analytical methods may be useful in studying the metastable rate and its resonant enhancement for chemical as well as other bio-molecular systems.

## 1 Introduction

We study the metastability, internal frequencies, activation mechanism, energy transfer, and the collective base-flipping in a mesoscopic DNA via resonance with specific electric fields. Our study shows that while the mesoscopic DNA is metastable and robust to environmental effects, it is vulnerable to certain frequencies that could be targeted by specific THz fields for triggering its collective base-flipping dynamics and causing large amplitude separation of base pairs.

THz radiation (0.1 THz to 10 THz) lies between the infrared and microwave regions and is non-ionizing. And the mechanisms by which it interacts with cells and tissues are fundamentally different from those involved in interactions of living matter with high-energy ionizing radiation that cause damage by directly breaking covalent bonds in DNA and other biomolecules [43].

Since THz field is a frontier area for research in physics, chemistry, biology, material science and medicine, their impact on DNA dynamics is an extremely important question. In their study of DNA breathing dynamics in the presence of a THz field – based on the PBD model [10] with a drag term and a harmonic driving force, Alexandrov et al. [2] argued that a specific THz radiation exposure may significantly affect the natural dynamics of DNA, and thereby influence intricate molecular processes involved in gene expression and DNA replication. Lots of controversy follow: some considered their paper excellent while others saw it as "physically unrealistic" [40, 28].

Titova et al. [41, 42, 43] brought the interest to another level. They demonstrated in vitro, and in vivo that intense (220 kV/cm), picosecond, THz pulses with 1 KHz repetition rate can elicit cellular molecular changes in exposed skin cells and tissues in absence of thermal effects. They observed that exposure to intense THz pulses (i) leads to a significant induction of H2AX phosphorylation which indicates DNA damage, and at the same time an increase in several proteins which suggest that DNA damage repair mechanisms are quickly activated, (ii) causes favorable changes in the expression of multiple genes implicated in inflammatory skin diseases and skin cancers which suggests potential therapeutic

applications of intense THz pulses. Moreover, they pointed out that (iii) the low average power of THz pulse sources in their experiment results in biologically insignificant temperature increases of only fractions of a degree at most, (iv) but the high energy density per pulse produces peak powers and corresponding electric fields that can be extremely high and it is likely that these high peak electric fields are responsible for the observed THz-pulse-driven cellular effects <sup>1</sup>.

In their papers, they also mentioned the work of Alexandrov et al. in a favorable light and hoped to understand better the mechanisms, and the specific requirements for the intensity and frequency of the radiation.

## 1.1 A New DNA Model with Environmental Effects and Radiation

Building on our earlier work on DNA [25], the insights from this controversy, and especially the non-thermal experimental results of Titova et al., we develop a new mesoscopic DNA model in Section 2 of this paper that takes into account not only the issues of helicity and the coupling of an electric field with the base dipole moments, but also includes the environmental effects such as fluid viscosity and thermal noise [18, 45, 44, 46, 29]. Moreover, all the parameter values are chosen to best represent the typical values for the opening and closing dynamics of a DNA [7, 11].

We start with a mesoscopic DNA in the fluid with thermal noise, but disregard the additional thermal effects by ignoring radiation-fluid interactions (i.e., in the non-thermal regime), in order to focus our attention mainly on the effects of radiation on the DNA via coupling the electric field with the DNA bases. The new mesoscopic DNA model allows us to employ Freidlin-Wentzell theory of stochastic averaging [22, 20, 21, 19, 39] and the newly developed theory of resonant enhancement [9, 16, 36, 15]. Our study in Section 3 and Section 4 shows that while the mesoscopic DNA is metastable and robust to environmental effects, it is vulnerable to certain frequencies that could be targeted by specific THz fields for triggering its collective base-flipping dynamics and causing large amplitude separation of base pairs.

## 1.2 The Mesoscopic DNA is Robust Against Noise

To determine whether the mesoscopic DNA is robust to noise and will survive in a normal environment without radiation, we estimate its mean life span,  $T_{DNA}$ , where the base pairs have not gone through a collective base-flipping and have not had a large amplitude separation, due to environmental random perturbations.

For our study,  $T_{DNA}$  is nothing but the mean first passage time (MFPT) for the 2N-dimensional diffusion process defined by the kinetic Langevin system of our model, namely, Eq.(5) with  $\mathcal{E} = 0$ , i.e., without radiation. In order

---

<sup>1</sup>See Section 4.3 for more details on the experiments of Titova et al. and the discussion of the issue of waves vs pulses.

to estimate this  $\text{MFPT}_{2N}$ , we proceed as follows in Section 3 : (1) we set up the MFPT equation for this  $2N$ -dimensional Hamiltonian diffusion process with weak noise; (2) we use Freidlin-Wentzell method of Hamiltonian stochastic averaging to reduce the above equation to a MFPT equation for an 1D energy diffusion process defined on a graph; (3) we simplify and use Monte Carlo numerical methods to obtain the drift and diffusion coefficients for this stochastic averaged equation; and (4) we solve this stochastic averaged equation and obtain an approximation of the  $\text{MFPT}_{2N}$  for the full  $2N$ -dimensional diffusion process. As it turns out, the mean first passage time of our mesoscopic DNA,  $\text{MFPT}_{2N}$ , is equal to  $6.1487 \times 10^{18}$  picoseconds from our semi-analytical computation.

Hence,  $T_{DNA} = 6.1487 \times 10^{18}$  ps which is about 10 weeks. Since the mean life time of a skin cell is about 2 to 4 weeks, and  $T_{DNA} > T_{cell}$ , we can reasonably conclude that the mesoscopic DNA is robust against noise and will survive in a normal environment without radiation.

### 1.3 But It is Vulnerable to Specific THz Fields

After showing that the mesoscopic DNA is robust against noise, we try to quantify the requirements for specific electric fields that can trigger its collective base-flipping dynamics and cause large amplitude separation of base pairs. We use the newly developed theory of resonant enhancement of the rate of metastable transition [9], which has been built on the work of large deviation theory [22] and the results of researches in physics [16, 36, 15].

In Section 4, we first briefly summarize the main results of this new theory of resonant enhancement and then apply it to our mesoscopic DNA model. And we find the requirements for the specific electric fields in the following steps: (1) we obtain numerically the most probable path (MPP) which is essentially the heteroclinic connection between the metastable equilibrium point at the bottom of the left potential well and the rank-one saddle; (2) we derive analytically the formula for the work done by the electric field along the MPP that winds from the bottom to the top of the potential well; (3) we use this formula to find, via numerical methods, the requirements for the specific electric fields and conclude that the mesoscopic DNA is vulnerable to THz fields with frequencies around 0.28 THz and with amplitudes in the order of 450 kV/cm.

These estimates compare well with the experimental data of Titova et al. [41, 42, 43], which have demonstrated that they could affect the function of DNA in human skin tissues by THz pulses with frequencies around 0.5 THz and with a peak electric field at 220 kV/cm. Moreover, our estimates also conform to a number of other experimental works [34, 24, 1] which appeared in the last couple years.

### 1.4 The Need to Model THz Pulses

But more study is needed to take into consideration the issue of modeling the pulses. In the experiments of Titova et al., they skillfully used intense THz pulses with low repetition rate to obtain a sufficiently high peak electric field and

to affect the DNA function in a non-thermal setting. In our present study, we try to theoretically investigate the mechanisms and requirements for such radiation using the existing tools in the field of control of stochastic mechanical systems. By ignoring the additional radiation-fluid interaction, we get ourselves into the non-thermal setting, minimize the impacts of the issue of waves vs pulses, and enable us to obtain some interesting and important results. And we wish that future research will extend the present theory of resonant enhancement to the case where the radiation are pulses. However, even as it stands right now, our new DNA model and semi-analytical estimates may have suggested resonance as a possible mechanism for these experimental results and hopefully will inspire new experimental designs that may settle this issue.

Moreover, we believe that our semi-analytical methods may be useful in studying the metastable rate and its enhancement for chemical as well as other bio-molecular systems.

## 2 A New DNA Model with Environmental Effects and Radiation

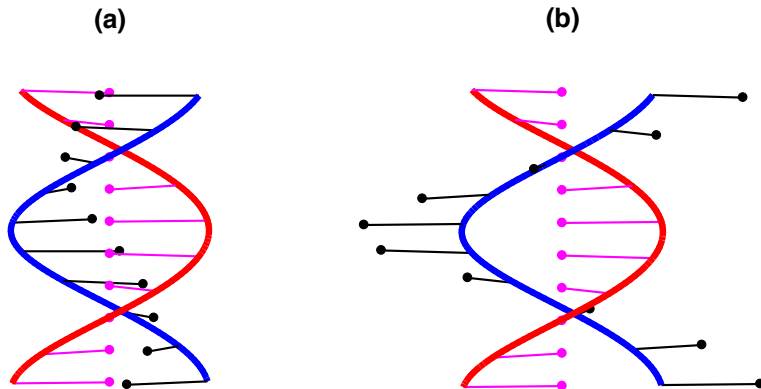


Figure 1: A model of DNA opening dynamics with 10 pendula (for illustration only, but  $N = 30$  throughout this paper). The work of Yomosa has shown us how to generalize the model of Englander et. al. to a helical model simply by twisting both strands forward by  $36^\circ$ . The system has two global stable equilibria, achieved when all the pendula (in black color) have the same angular displacements  $\theta_n = \theta_e$  and each is positioned at the equilibria of a single pendulum. Figure (a) shows the case where  $\theta_e = -2.6906$  (left equilibrium point in Figure (2)). (b) The system also has a rank one saddle at  $\theta_n = 0$  (and  $p_{\theta_n} = 0$ ) where all pendula (in black color) are at the outward position. For a small energy, the pendula are librating near one of the global stable equilibria where all angles  $\theta_n$  are the same and equal to  $\theta_e$ . For a large enough energy, the pendula will move collectively from one energy basin to the other and flip across the rank one saddle.

## 2.1 The Torsional Model of DNA Opening Dynamics

The torsional model [18, 45] is a chain of equivalent pendula (in black color) that rotate about the axis of a fixed backbone with an angle  $\theta_n$  measured from the outward position. The pendula interact with nearest neighbors along the backbone through harmonic torsional coupling, and with pendula (in pink color) on the opposing immobilized strand through a Morse potential that has two stable equilibria and a saddle. See Figure (1) and Figure (2).

### 2.1.1 Brief Remarks on the History of the Torsional Model

In a pioneering paper [18], biophysicists Englander et al. first modeled the DNA as a double chain of coupled pendula, and employed it to investigate the base pair opening and motion of transcription bubble. Many researchers built on this torsional model. Yomosa [45] generalized it to a helical model by twisting both strands forward by  $36^\circ$ . Russian biophysicist Yakushevich extended it in a series of papers, making it an excellent first model in exploring the DNA opening dynamics and transcription [44]. More recently, Mezic, as well as others, used it in studying the structural activation of large-amplitude collective motions of the bases [29, 14, 17, 25].

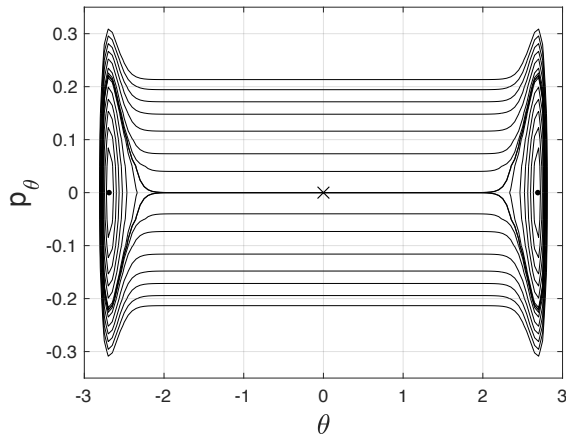


Figure 2: The phase space  $(\theta, p_\theta)$  of a single pendulum in a Morse potential and without torsional coupling with its nearest neighbors. It has two stable equilibria and a saddle. The curve containing the saddle at  $(0, 0)$  is a homoclinic orbit that separates two types of motion, namely, the libration near the equilibria  $(\theta_e, 0) = (\pm 2.6906, 0)$ , and the flipping across the saddle  $(0, 0)$ .

In a related but different direction, other researchers studied the models for the radial stretching motions of DNA molecule, which are related in particular to DNA thermal denaturation. The main line of research in this direction followed

the formulation of Peyrard-Bishop-Dauxois model [32, 10], which Alexandrov et al. used in exploring the effects of a THz field on the DNA breathing dynamics [2].

### 2.1.2 The Hamiltonian for the DNA Opening Dynamics

The Hamiltonian that describes the motion of these  $N$  coupled pendula is given by

$$H_0(\theta, P_\theta) = \sum_{n=1}^N \left[ \frac{P_{\theta_n}^2}{2I} + \frac{1}{2}S(\theta_n - \theta_{n-1})^2 + D \left( e^{-a_d\{l(1+\cos\theta_n)-x_0\}} - 1 \right)^2 \right] \quad (1)$$

with periodic boundary condition,  $\theta_0 = \theta_N$ .  $N = 30$  for this study. The first term is the kinetic energy terms of the  $N$ -pendula. The second term is the torsional coupling terms. The third term is the Morse potential terms, which model the hydrogen bonds of the respective DNA base pairs. In Eq. (1),  $P_{\theta_n} = I(d\theta_n/dt')$  is the generalized momentum conjugate to  $\theta_n$  where  $t'$  is the natural time of the model. All the parameter values are chosen to best represent the typical values for the opening and closing dynamics of DNA [7, 11] and are given as follows:

1. The parameter  $I$  represents the moment of inertia of each pendulum and is given by  $I = 18600 \times 1.67 \times 10^{-47} \text{ kg} \cdot \text{m}^2 = 310.62 \text{ pN} \cdot \text{nm} \cdot \text{ps}^2$ .
2. The parameter  $S$  determines the strength of the nearest neighbor coupling and is given by  $S = 2 \text{ eV} = 320.4 \text{ pN} \cdot \text{nm}$ .
3. The parameter  $D$  determines the strength of the Morse potential and is given by  $D = 0.05 \text{ eV} = 8.01 \text{ pN} \cdot \text{nm}$ .
4.  $x_0$ ,  $a_d$ , and  $h$  represent the equilibrium distance, the width of the Morse potential, and the length of each pendulum, respectively. Their values are given by  $x_0 = 0.1 \text{ nm}$ ,  $a_d = 19 \text{ nm}^{-1}$ , and  $l = 1 \text{ nm}$ .

After dividing both sides of Eq. (1) by  $S$ , the Hamiltonian can be non-dimensionalized as

$$H(\theta, p_\theta) = \sum_{n=1}^N \left[ \frac{1}{2}p_{\theta_n}^2 + \frac{1}{2}(\theta_n - \theta_{n-1})^2 + \kappa \left( e^{-a(1+\cos\theta_n-d_0)} - 1 \right)^2 \right] \quad (2)$$

where  $p_{\theta_n} \equiv d\theta_n/dt$  is the dimensionless momentum defined with respect to the dimensionless time  $t = \sqrt{S/I} t'$ . Thus, in this study, one unit time ( $t = 1$ ) corresponds to  $t' = \sqrt{I/S} = 0.9846 \text{ ps}$ . In Eq. (2), the dimensionless amplitude of the Morse potential  $\kappa$  is a small parameter and is given by  $\kappa = D/S = 0.025$ . We have also introduced the dimensionless decaying coefficient of Morse potential  $a \equiv a_d l = 19$ , and the dimensionless equilibrium distance  $d_0 \equiv a_d x_0 / a = 0.1$ .

### 2.1.3 Libration and Collective Base-Flipping

Before studying the dynamics of this N-pendula torsional model, it is instructive to look at a single pendulum in a Morse potential without coupling. Figure (2) shows the phase space of such single pendulum. It has two stable equilibria and a saddle. The curve containing the saddle  $(0, 0)$  is a homoclinic orbit that separates two types of motion, namely, the oscillation near the equilibria  $(\theta_e, 0) = (\pm 2.6904, 0)$ , and the flipping across the saddle  $(0, 0)$ . The N-coupled pendula have similar but much more complicated behaviors. First, the system has two global stable equilibria, achieved when all the pendula have the same angular displacements  $\theta_n = \theta_e$  (thus nullifying the nearest neighbors coupling) and each is positioned at the equilibria of a single pendulum. It also has a rank one saddle at  $\theta_n = 0$  (and  $p_{\theta_n} = 0$ ) where all pendula are at the outward position. For a small energy, the pendula are librating near one of the global stable equilibria where all angles  $\theta_n$  are the same and equal to  $\theta_e$ . For a large enough energy, the pendula will move collectively from one energy basin to the other and to flip across the rank one saddle. Numerical simulations show that the minimum activation energy for flipping depends on the way how the energy is injected [14, 17, 25].

## 2.2 Equations of Motion for the New DNA Model

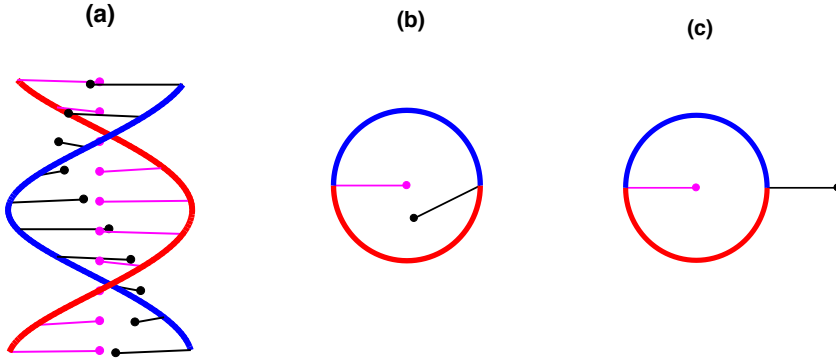


Figure 3: Figure (a) shows the DNA model at its left global equilibrium point where  $\theta_n = \theta_e = -2.6906$ . Figure (b) shows the positions of the first base pair at the global left equilibrium point, with pink one immobilized and black one at  $\theta_e = -2.6906$ . The work of Zhang provides us with the idea of coupling an electric field with the dipole moments of DNA bases. If we assume that the electric field is perpendicular to the DNA central axis and is directed to the inverted direction of the first base shown in Figure (c), then the moment of force exerted on the  $n$ -th base can be written as  $T_n = -P_n \sin(\theta_n + (n - 1)\pi/5) E \cos \Omega_0 t'$ .

The new DNA model, as anticipated in our previous paper [25], will take



into account the issues of (i) helicity, (ii) coupling of an electric field with the base dipole moments, and (iii) environmental effects of fluid viscosity and thermal noise. It will allow us to explore the possibility, the requirement, and the mechanism for an electric field to trigger its collective base-flipping dynamics, cause large amplitude separation of base pairs, and disrupt the function of DNA<sup>2</sup>.

### 2.2.1 The Coupling of an Electric Field with the Bases of a DNA

As mentioned earlier, the work of Yomosa [45] has showed us how to generalize the model of Englander et al. to a helical model simply by twisting both strands forward by  $36^\circ$ . And the work of Zhang [46] provides us with the idea of coupling an electric field with the dipole moments of DNA bases. If we assume that the electric field is perpendicular to the DNA central axis and is directed to the inverted direction of the first base, then the moment of force exerted on the  $n$ -th base can be written as

$$T_n = -P_n \sin(\theta_n + (n-1)\pi/5) E \cos \Omega_0 t' \quad (3)$$

where  $E, \Omega_0$  are the amplitude and the angular frequency of the electric field, and  $P_n$  is the dipole moment of the  $n$ -th base. The helical geometry requires the  $\pi/5$  twisting. See Figure (3). Below, for convenience, we will ignore the negative sign in Eq. (3) simply by modifying the electric field by half of a cycle.

Moreover, since the model is homogeneous in this paper, we will assume that  $P_n = P$  from now on where  $P$  is the average dipole moment taken from the work of Zhang. As for the issue of inhomogeneity, our initial computations have convinced us that the frequencies and amplitudes of the required fields for triggering the collective base-flipping are definitely sequence dependent (A,T,G,C), but we will leave them to our next paper.

### 2.2.2 The Inclusion of Environmental Effects

After including environmental effects [5, 27, 30], the new model can be seen as a periodically-driven kinetic Langevin system for the torsional model:

$$\begin{aligned} d\theta_n &= I^{-1} P_{\theta_n} dt' \\ dP_{\theta_n} &= S(\theta_{n+1} - 2\theta_n + \theta_{n-1}) dt' - DU'_0(\theta_n) dt' - \gamma I^{-1} P_{\theta_n} dt' \\ &\quad + F \sin(\theta_n + (n-1)\pi/5) (\cos \Omega_0 t') dt' + \sqrt{2\beta_0^{-1} \gamma} dW \end{aligned} \quad (4)$$

where  $n = 1, \dots, N$ ,  $\theta_0 = \theta_N$ ,  $U'_0$  is the derivative of the Morse potential  $U_0$ . It can be non-dimensionalized as

$$\begin{aligned} d\theta_n &= p_{\theta_n} dt \\ dp_{\theta_n} &= (\theta_{n+1} - 2\theta_n + \theta_{n-1}) dt - \kappa U'(\theta_n) dt - \nu \kappa p_{\theta_n} dt \\ &\quad + \mathcal{E} \kappa \sin(\theta_n + (n-1)\pi/5) (\cos \Omega t) dt + \sqrt{2\beta^{-1} (\nu \kappa)} dW \end{aligned} \quad (5)$$

<sup>2</sup>We will consider the coupling of an electric field with the base dipole moments, but will ignore the additional temperature effect induced by the radiation-fluid interaction. See Section 4.3 for more details.

where  $U'$  is the derivative of the non-dimensional Morse potential  $U$ . As for the parameters of these two systems, they are related as follows:

1.  $\gamma I^{-1}$  is the frictional coefficient which models the damping of the collective base rotation inside the DNA by the surrounding fluid molecules:  $\nu\kappa = \gamma I^{-1} \sqrt{I/S}$ . Usually, it is defined via the time of relaxation and is in the order of 100 ps [35, 44]. In this work, we set  $t'_r = 150$  ps. Hence

$$\nu\kappa = \frac{1}{150 \text{ (ps)}} (\sqrt{I/S}) = 0.006564 \quad (6)$$

and the system is underdamped.

2.  $\beta_0^{-1}$  is the Boltzmann temperature which models the thermal energy gain:  $k_B T = \beta_0^{-1} = S\beta^{-1}$  where  $k_B$  is the Boltzmann constant and  $T$  is the absolute temperature. For body temperature,  $T = 273 + 37 = 310$  K, and  $\beta^{-1}$  is given by

$$\beta^{-1} = k_B T / S = 4.2811 \times 10^{-21} \text{ J} \times 6.242 \times 10^{18} \text{ (eV)/J} / (2 \text{ eV}) = 0.01336$$

3.  $F = P \cdot E$  is the amplitude of the excitation which models the moment of force exerted on DNA base by the electric field:  $PE = \mathcal{E}\kappa S$ . For average dipole moment, we set  $P = 5.3$  db [46]. And the electric field amplitude is given by

$$E = \frac{8.01 \times \mathcal{E}}{0.3356 \times 10^{-8} \times P} \text{ (V/m)} = 4503.3 \times \mathcal{E} \text{ (kV/cm)} \quad (7)$$

Here, It is interesting to note that if  $\mathcal{E}$  is in the order of 0.1, then  $E$  will be in the order of 400 kV/cm as in the experiments of Titova et al. [41, 42, 43]. See Section 4.3.

4.  $\Omega_0$  and  $\Omega$  are the angular frequencies of excitation in the respective system:  $\Omega_0 = \Omega \sqrt{S/I}$  (radian/ps). Hence, the resonant frequency

$$\Omega_0 / 2\pi = 1.0156 \times \Omega / 2\pi \text{ (rev/ps} = \text{THz)}. \quad (8)$$

If the non-dimensional  $\Omega$  is in the order of 1, then the resonant frequency will be in the order of 0.1 THz and can be considered as a THz field.

### 2.3 Robust Against Noise But Vulnerable to Specific THz Fields?

After developing a new helical DNA model that takes into consideration all the relevant issues such as fluid and radiation, and selecting the parameter values that best represent the typical data for the opening and closing dynamics of a DNA, we are ready to explore the possibility, the requirement, and the mechanism for a electric field to trigger its collective base-flipping dynamics,

causing large amplitude separation of base pairs, and disrupting the function of DNA.

But before we start, we need to first check that our mesoscopic DNA is robust against noise when there is no radiation, i.e., when  $\mathcal{E} = 0$ . Since the forceless system is a kinetic Langevin system with weak noise, we can quantify the metastability of its normal state where the pendula librate near its equilibrium point, via Freidlin-Wentzell method of Hamiltonian stochastic averaging. And we need to determine whether the mean life span of our mesoscopic DNA – where the base pairs have not gone through a collective base-flipping and have not had a large separation of base pairs due to environmental perturbations, is sufficiently long enough so that we can have confidence that it will survive in a normal environment without radiation.

In Section 3, we will answer the question: "is the mesoscopic DNA robust against noise?" In Section 4, we will deal with the issue: "is it vulnerable to specific THz fields?".

### 3 The Mesoscopic DNA is Robust Against Noise

To determine whether the mesoscopic DNA is robust to noise and will survive in a normal environment without radiation, we estimate its mean life span,  $T_{DNA}$ , due to environmental random perturbations, where the base pairs have not gone through a collective base-flipping and have not had a large amplitude separation. For the rest of the paper, we will call it the mean life span of collective base-flipping and use it to mark the life span of our mesoscopic DNA.

For our study,  $T_{DNA}$  is nothing but the mean first passage time (MFPT) for the  $2N$ -dimensional diffusion process defined by the kinetic Langevin system of our model, Eq. (5) with  $\mathcal{E} = 0$ , i.e., without radiation. In order to estimate this  $\text{MFPT}_{2N}$ , we will proceed as follows: (1) we will set up the MFPT equation for this  $2N$ -dimensional Hamiltonian diffusion process with weak noise; (2) we will use the Freidlin-Wentzell method of Hamiltonian stochastic averaging to reduce the above equation to a MFPT equation for an 1D energy diffusion process defined on a graph; (3) we will simplify and use Monte Carlo numerical methods to obtain the drift and diffusion coefficients for this stochastic averaged equation; and (4) we will solve this stochastic averaged equation and obtain an approximation of the  $\text{MFPT}_{2N}$  for the full  $2N$ -dimensional diffusion process.

As it turns out, our semi-analytical estimations in this section will show that the mean life span of collective base-flipping of the mesoscopic DNA,  $T_{DNA}$ , is equal to  $6.1487 \times 10^{18}$  ps, which is about 10 weeks long. Since the life time of a skin cell is between 2 to 4 weeks, and  $T_{DNA} > T_{cell}$ , we can reasonably conclude that the mesoscopic DNA is robust against noise and will survive in a normal environment without radiation. Moreover, a closer analysis of these estimates will also allow us to remark that FW theory is essential in studying the MFPT and its corresponding metastable rate.

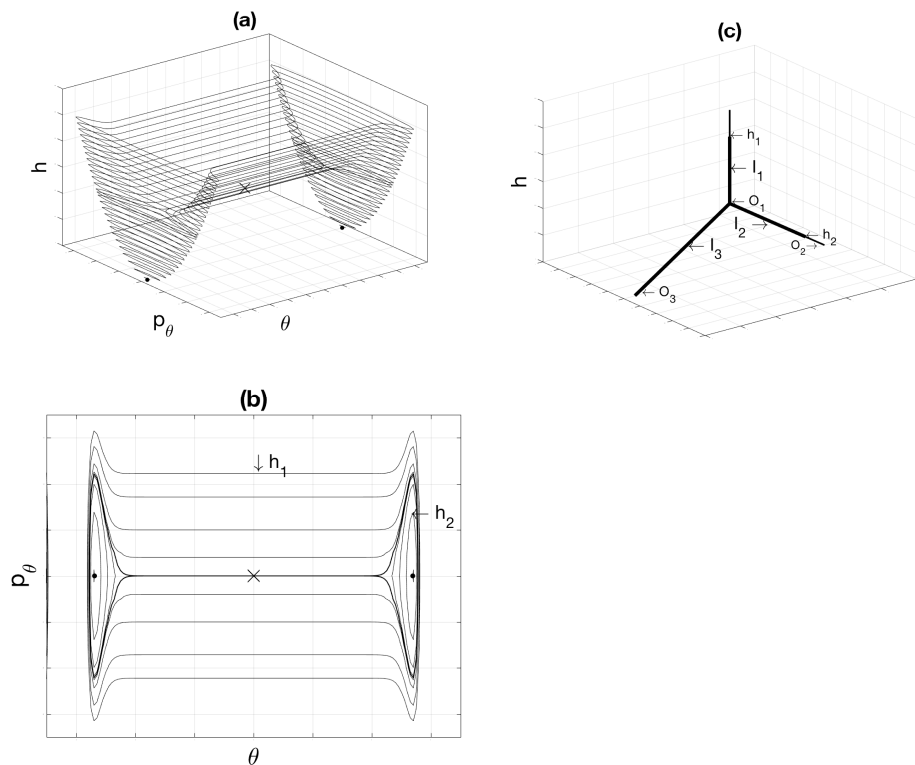


Figure 4: These figures are for conceptual illustrations only. (a) A  $(2N + 1)$ -dimensional Hamiltonian contour plot with Figure (b) as its corresponding  $2N$ -dimensional version. See references [21, 22] for the geometry of Hamiltonian systems with many degrees of freedom. (b)  $G$  is a bounded region in the  $2N$ -dimensional space  $(\theta, p_\theta)$  with the boundary  $\partial G = \partial G_2 \cup \partial G_1$ , where  $\partial G_2 = \{(\theta, p_\theta) : H(\theta, p_\theta) = h_2 \text{ \& } \theta > 0\}$  is a energy level set blocking away a small neighborhood of the bottom of the right well.  $\partial G_1 = \{(\theta, p_\theta) : H(\theta, p_\theta) = h_1\}$  is another appropriately chosen energy level set with its energy higher than the energy of the rank-one saddle. (c) Graph  $\Gamma$  is homeomorphic to the set of connected components of level sets of  $H(\theta, p_\theta)$ .  $\Gamma$  consists 3 edges,  $I_1, I_2, I_3$ , with  $I_3, I_2$  corresponding to those in the left and right well respectively, and with  $I_1$  corresponding to those above the saddle.  $\Gamma$  also has 3 vertices, with  $O_2, O_3$  corresponding to two equilibria, and  $O_1$  corresponding to the energy level set containing the rank-one saddle.

### 3.1 MFPT for a 2N-dim. Hamiltonian Diffusion with Weak Noise

Let  $G$  be a bounded region in  $R^{2N}$  with the smooth boundary  $\partial G = \partial G_2 \cup \partial G_1$ , where  $\partial G_2$  is an energy level set blocking away a small neighborhood of the bottom of the right well,  $\partial G_1$  is another appropriately chosen energy level set with its energy higher than the energy of the rank-one saddle. See Figure (4) for illustrations. Then, the MFPT<sub>2N</sub>,  $\tilde{m}^\epsilon(q_0, p_0)$ , from a point  $(q_0, p_0)$  near the bottom of the left well can be computed by solving the following Dirichlet problem<sup>3</sup>:

$$\begin{aligned}\tilde{L}^\epsilon \tilde{m}^\epsilon(q, p) &= -1, & (q, p) \in G \\ \tilde{m}^\epsilon(q, p) &= 0, & (q, p) \in \partial G\end{aligned}\tag{9}$$

where  $\tilde{L}^\epsilon$  is the differential operator corresponding to the kinetic Langevin system (Eq. (5) with  $\mathcal{E} = 0$ ). And the metastable rate is just the inverse of  $\tilde{m}^\epsilon(q_0, p_0)$ .

However, this partial differential equation is extremely difficult, or perhaps impossible to solve, even numerically. Fortunately, Freidlin-Wentzell Theory of Random Perturbations of Hamiltonian Systems allows us to reduce this difficult problem to something more manageable, namely, by solving a corresponding Dirichlet problem, a linear ODE, on a subset  $\Gamma_G (= Y(G))$  of a graph  $\Gamma$ . See Eq. (10) in Section 3.2.3.

### 3.2 MFPT for a Stochastic Averaged 1D Energy Diffusion on a Graph

Notice that this kinetic Langevin system is underdamped (see Eq. (6)), has a Hamiltonian  $H(q, p)$  that is its only first integral, and has two stable equilibria and a rank-one saddle. Its long time behavior can be described by a diffusion process on a graph. Inside each edge, the process is defined by the standard average procedure, but for the whole process, a gluing condition is needed at an interior vertex corresponding to the energy level set that contains the rank-one saddle. The differential operator of this energy process can be used to set up a Dirichlet problem on the graph whose solution can be used to approximate the MFPT for the original problem. See references [22, 20, 21, 19, 39] for details. However, since these materials scatter in many publications, for the convenience of readers, we will summarize below the most relevant ones, make them applicable to our problem, and with similar notations used in the book by Freidlin and Wentzell [22]<sup>4</sup>.

<sup>3</sup>Note: for mathematicians, Eq. (9) is a Dirichlet problem; for scientists and engineers, a Pontryagin equation, and for this paper, the term, MFPT equation, will also be used in certain situations.

<sup>4</sup>For example: we will use  $(q, p)$  instead of  $(\theta, p_\theta)$ ;  $\epsilon$  instead of  $\nu\kappa$ , etc.

Given the DNA equations without the electric field

$$\begin{aligned}\dot{\tilde{q}}_t^\epsilon &= \nabla_p H(\tilde{q}_t^\epsilon, \tilde{p}_t^\epsilon), \\ \dot{\tilde{p}}_t^\epsilon &= -\nabla_q H(\tilde{q}_t^\epsilon, \tilde{p}_t^\epsilon) - \epsilon \nabla_p H(\tilde{q}_t^\epsilon, \tilde{p}_t^\epsilon) + \sqrt{2\beta^{-1}\epsilon} \dot{W}_t\end{aligned}$$

Even though the perturbation is degenerate, the system is kinetic Langevin and hence hypo-elliptic and the theory of Hörmander is applicable [6, 31]. As in the case of non-degenerate perturbations, the process  $(\tilde{q}_t^\epsilon, \tilde{p}_t^\epsilon)$  in  $R^{2N}$  has, roughly speaking, fast and slow components. The fast component corresponds to the motion along the non-perturbed trajectories on a connected component of a  $R^{2N-1}$ -dimensional energy surface. The slow component corresponds to the motion transversal to the same connected component. Moreover, the fast component can be characterized by the invariant density of the non-perturbed system on the corresponding connected component.

To study the slow component, we rescale the time: put  $q_t^\epsilon = \tilde{q}_{t/\epsilon}^\epsilon, p_t^\epsilon = \tilde{p}_{t/\epsilon}^\epsilon$ . Then  $(q_t, p_t)$  satisfies equations

$$\begin{aligned}\dot{q}_t^\epsilon &= \frac{1}{\epsilon} \nabla_p H(q_t^\epsilon, p_t^\epsilon), \\ \dot{p}_t^\epsilon &= -\frac{1}{\epsilon} \nabla_q H(q_t^\epsilon, p_t^\epsilon) - \nabla_p H(q_t^\epsilon, p_t^\epsilon) + \sqrt{2\beta^{-1}} \dot{W}_t\end{aligned}$$

where  $W_t$  is a  $N$ -dimensional Wiener process.

### 3.2.1 Standard Stochastic Averaging for Diffusion in One Well

First, we restrict our attention only to the left well. Then the slow component of the process can be characterized by how the energy Hamiltonian  $H(q_t^\epsilon, p_t^\epsilon)$  changes. Using Ito formula, we have

$$\begin{aligned}H(q_t^\epsilon, p_t^\epsilon) - H(q_0, p_0) &= \sqrt{2\beta^{-1}} \int_0^t \nabla_p H(q_s^\epsilon, p_s^\epsilon) \cdot dW_s \\ &+ \beta^{-1} \int_0^t \Delta_p H(q_s^\epsilon, p_s^\epsilon) ds - \int_0^t \nabla_p H^*(q_s^\epsilon, p_s^\epsilon) \nabla_p H(q_s^\epsilon, p_s^\epsilon) ds\end{aligned}$$

Applying the standard averaging procedure with respect to the invariant density of the fast motion, with the slow component frozen, the processes  $Y_t^\epsilon = H(q_t^\epsilon, p_t^\epsilon)$  converges weakly in the space of continuous function to the diffusion process  $Y_t$ , whose operator is given below by

$$L = \beta^{-1} \frac{u(h)}{v(h)} \frac{d^2}{dh^2} + \beta^{-1} \frac{w(h)}{v(h)} \frac{d}{dh} - \frac{u(h)}{v(h)} \frac{d}{dh}$$

where

$$\begin{aligned}
u(h) &= \oint_{C(h)} \nabla_p H^*(q, p) \nabla_p H(q, p) \frac{dS}{|\nabla H(q, p)|} \\
w(h) &= \oint_{C(h)} \Delta_p H(q, p) \frac{dS}{|\nabla H(q, p)|} = \frac{d}{dh} u(h) \\
v(h) &= \oint_{C(h)} \frac{dS}{|\nabla H(q, p)|}
\end{aligned}$$

Here,  $\frac{\text{const.}}{|\nabla H(q, p)|}$  is the invariant density with respect to the volume on the energy surface  $C(h) = \{(q, p) \in R^{2N} : H(q, p) = h\}$ ;  $dS$  is the surface element on  $C(h)$ . The point 0 which corresponds to the stable equilibrium point in the left well is an exterior vertex and hence inaccessible for the process  $Y_t$ . For the proof of  $w(h) = u'(h)$ , see Appendix A.1.

### 3.2.2 FW Theory for Diffusion in Space with Multiple Wells

For computing the MFPT and the metastable rate, we need to consider the whole phase space, in order to keep track of all the trajectories that start from the bottom of the left well, diffuse across the saddle, and reach the neighborhood of the bottom of the right well. In this case, level sets of the Hamiltonian may have more than one component. Consider now the graph  $\Gamma$  homeomorphic to the set of connected components of level sets of  $H(q, p)$ . Then,  $\Gamma$  will consist 3 edges,  $I_1, I_2, I_3$  and 3 vertices  $O_1, O_2, O_3$ . Let  $Y : R^{2N} \rightarrow \Gamma$  be this mapping.  $Y(q, p)$  is a point of  $\Gamma$  corresponding to the connected components of  $C(H(q, p))$  containing point  $(q, p) \in R^{2N}$ , and  $Y(q, p) = (i(q, p), H(q, p))$ , where pair  $(i, H)$  forms the coordinates on  $\Gamma$ . Consider random processes  $Y_t^\epsilon = Y(q_t^\epsilon, p_t^\epsilon)$  on  $\Gamma$ . These processes converge weakly to the diffusion process  $Y_t$  on  $\Gamma$ . To calculate the characteristics of the limiting process, consider, first, the interior  $(i, h)$  of the edge  $I_i \subset \Gamma$ . Let  $C_i(h)$  be the corresponding level set component. As before, the process  $Y_t$  inside  $I_i$  is governed by the operator

$$L_i = \frac{2\beta^{-1}}{v_i(h)} \frac{d}{dh} \left( \frac{u_i(h)}{2} \frac{d}{dh} \right) - \frac{u_i(h)}{v_i(h)} \frac{d}{dh}$$

To determine the limiting process for all  $t > 0$ , the behavior of the process at the vertices, namely, the exterior vertices,  $O_3$  of  $I_3$  ( $O_3 \sim I_3$ ) and  $O_2$  of  $I_2$  ( $O_2 \sim I_2$ ), and the interior vertex  $O_1$  which connects 3 edges  $I_1, I_2, I_3$  ( $I_3 \sim O_1, I_2 \sim O_1, O_1 \sim I_1$ ), need to be described.

### 3.2.3 MFPT for 1D Energy Diffusion Process on a Graph

With this differential operator of  $Y_t$  in hand, we can use Freidlin-Wentzell another result that

$$\lim_{\epsilon \rightarrow 0} \epsilon \tilde{m}^\epsilon(q, p) = m(i(q, p), H(q, p))$$

to estimate the MFPT<sub>2N</sub>,  $\tilde{m}^\epsilon(q, p)$ , from the solution,  $m(i, h) = m_i(h)$ , of the following Dirichlet problem on  $\Gamma_G$ :

$$\begin{aligned} \frac{2\beta^{-1}}{v_i(h)} \frac{d}{dh} \left( \frac{u_i(h)}{2} \frac{dm_i(h)}{dh} \right) - \frac{u_i(h)}{v_i(h)} \frac{dm_i(h)}{dh} &= -1 \\ m_i(h) &= 0, \quad (i, h) \in \partial\Gamma_G. \end{aligned} \quad (10)$$

where

1.  $m(i, h)$  is continuous on  $\Gamma_G$ ;
2. the gluing condition is satisfied at the interior vertex  $O_1$ , i.e.,

$$\alpha_3 \frac{dm_3(h)}{dh} + \alpha_2 \frac{dm_2(h)}{dh} = \alpha_1 \frac{dm_1(h)}{dh}$$

with

$$\alpha_i = \oint_{C_i(Y^{-1}(O_1))} \nabla_p H^*(q, p) \nabla_p H(q, p) \frac{dS}{|\nabla H(q, p)|};$$

3. the exterior vertex,  $O_3$ , is an entrance and inaccessible.

### 3.3 Computation of Drift and Diffusion Coefficients via MC Method

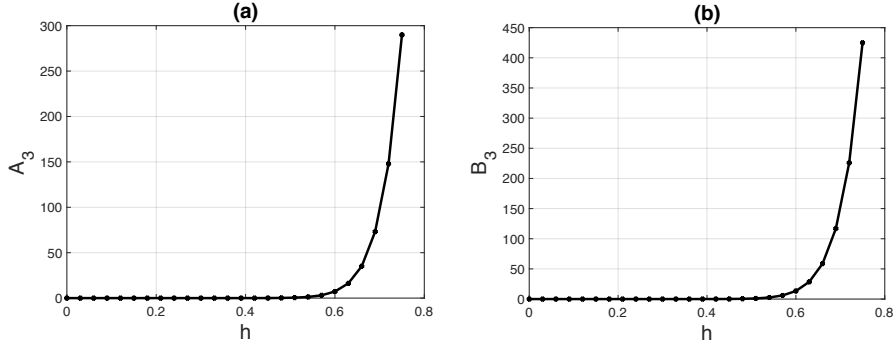


Figure 5: To compute the drift and diffusion coefficients for high DOF systems like DNA, we need to reduce the dimension of the volume integrals of  $u_i, v_i$  further by integrating  $dp' = dp_2 \dots dp_N$  part analytically first, and then employing the more sophisticated Metropolis Hastings Monte Carlo method to evaluate the remaining parts  $A_i, B_i$  given by Eq. (11). Figure (a) shows the coefficient  $A_3(h)$  as a graph of a function of  $h$  which is the energy coordinate on  $I_3$ . Similarly Figure(b) shows the graph for the coefficient  $B_3(h)$ . Moreover,  $A_1(h), A_2(h), B_1(h), B_2(h)$  can also be computed in the same way.



To solve this Dirichlet problem on  $\Gamma_G$ , Eq. (10), we need to employ numerical method to find its coefficients. But for high-dimensional system like DNA, we may need to do some simplification first.

(1) We will rewrite it compactly as

$$\frac{2\beta^{-1}}{v_i(h) e^{-\Psi_i(h)}} \frac{d}{dh} \left( e^{-\Psi_i(h)} \frac{u_i(h)}{2} \frac{dm_i(h)}{dh} \right) = -1$$

where  $\Psi_i(h) = \int^{h(I_i)} \frac{1}{\beta-1} dy$ .

(2) Since the surface of  $C_i(h)$  can be represented as a  $(2N - 1)$ -dimensional graph in  $R^{2N}$ , surface integrals for the coefficients,  $u_i(h), v_i(h)$ , can be transformed into volume integrals over the domains in the corresponding regions of the phase space [12, 13, 8]. For a few DOF systems, coefficients  $u_i, v_i$  can be computed from these volume integral formulas using simply the Monte Carlo method. But for high DOF systems like DNA, we need to reduce the dimension of the volume integrals further by integrating  $dp' = dp_2 \dots dp_N$  part analytically first [13], and then employing the more sophisticated Metropolis Hastings Monte Carlo method [4, 23] to evaluate the remaining parts  $A_i, B_i$  given below by:

$$\begin{aligned} A_i(h) &= \frac{1}{2} \int_{\Sigma_i(h)} (h - V(q))^{\frac{N}{2}} dq = u_i(h)/2c \\ B_i(h) &= \int_{\Sigma_i(h)} (h - V(q))^{\frac{N}{2}-1} dq = v_i(h)/c \end{aligned} \quad (11)$$

where  $\Sigma_i(h) = \{q : V(q) \leq h\}$ . See Appendix A.2 for more details for the derivation of Eq. (11).

(3) Figure (5) shows the coefficients,  $A_3(h), B_3(h)$ , as a graph of a function of the energy  $h$ , computed with the above method. Similarly,  $A_1(h), A_2(h), B_1(h)$  an  $B_2(h)$  can also be obtained in the same way, with the same geometric data of our DNA model collected below:

- bottom of the left well  $(\theta, p_\theta)$  where  $\theta_n = -2.6906$ ,  $p_{\theta n} = 0$ ,  $n = 1, \dots, N$ , and with energy  $h = 0$ ; bottom of the right well  $(\theta, p_\theta)$  where  $\theta_n = 2.6906$ ,  $p_{\theta n} = 0$  and with energy  $h = 0$ ;
- saddle  $(\theta, p_\theta)$  where  $\theta_n = 0$ ,  $p_{\theta n} = 0$ , and with energy level  $h = 0.75$ ;
- $\partial G_1$  is an energy level set with energy  $h_1 = 2.2$  which is much higher than the energy of the saddle;
- $\partial G_2$  is an energy level set with energy  $h_2 = 0.15$  which blocks away a small neighborhood of the bottom of the right well;
- hence, the energy coordinate  $h$  on  $I_3$  is from 0 to 0.75; the energy coordinate on  $I_2$  is from 0.15 to 0.75; the energy coordinate on  $I_1$  is from 0.75 to 2.2.

(4) If we set  $M_i = 2\beta^{-1}m_i$ , then the Dirichlet problem is now given by

$$\frac{1}{B_i(h) e^{-\Psi_i(h)}} \frac{d}{dh} \left( e^{-\Psi_i(h)} A_i(h) \frac{dM_i(h)}{dh} \right) = -1$$

$$M_i(h) = 0, \quad (i, h) \in \partial\Gamma_G \quad (12)$$

where

- $M_i(h)$  is continuous on  $\Gamma_G$ ;
- $M_i(h)$  satisfies the gluing condition at the interior vertex  $O_1$ ;

$$\alpha_3 \frac{dM_3(h)}{dh} + \alpha_2 \frac{dM_2(h)}{dh} = \alpha_1 \frac{dM_1(h)}{dh}$$

$$\alpha_i = A_i(h)|_{h=h_{O_1}}$$

- the exterior vertex,  $O_3$ , is inaccessible.

(5) Moreover, the MFET $_{2N}$ ,  $\tilde{m}^\epsilon(q, p)$ , is given by

$$\lim_{\epsilon \rightarrow 0} \epsilon \tilde{m}^\epsilon(q, p) = M(i(q, p), H(q, p))/2\beta^{-1}$$

and can be estimated by  $M(i(q, p), H(q, p))/2\beta^{-1}\epsilon$ .

### 3.4 Solutions for the 1D MFPT Equation on a Graph

After integrations over segments  $I_i$ , we obtain

$$M(i, h) = \int^{h(I_i)} \left[ \int^z -B_i(y) e^{-\Psi_i(y)} dy \right] \frac{2e^{\Psi_i(z)}}{A_i(z)} dz + b_i \int^{h(I_i)} \frac{2e^{\Psi_i(z)}}{A_i(z)} dz + c_i \quad (13)$$

with six constants of integration  $b_i, c_i$ . They can be determined uniquely by the following six conditions:

1. two boundary conditions at  $h_1, h_2$ ,
2. two continuous conditions at the interior vertex  $O_1$ ,
3. one gluing condition at the interior vertex  $O_1$ , and
4. one exterior vertex condition at  $O_3$ .

And their values are given below:

$$b_1 = 18.8310326781; \quad b_2 = 0.4189904781; \quad b_3 = 0$$

$$c_1 = 1.0944699430 \times 10^{15}; \quad c_2 = 0; \quad c_3 = 1.09446994586 \times 10^{15}$$

See Appendix A.3 for more details.

Moreover, if we denote the values of the first and second integration terms of Eq. (13) by  $-[[B]]^{h(I_i)}$  and  $[A]^{h(I_i)}$ , respectively, then the MFPT $_{2N}$ ,  $\tilde{m}^\epsilon(q_0, p_0)$ , that starts from a point  $(q_0, p_0)$  near the bottom of the left well and exits at the boundary  $\partial_2$  of the left well can be approximated by  $M_3(h(O_3)^+)/ (2\beta^{-1}\nu\kappa)$  where

$$\begin{aligned} M_3^\epsilon(h(O_3)^+)/ (2\beta^{-1}\nu\kappa) &= (-[[B_3]]_{h(O_3)^+}^{h(O_3)^+} + c_3)/ (2\beta^{-1}\nu\kappa) = c_3/ (2\beta^{-1}\nu\kappa) \\ &= 6.244878692881616 \times 10^{18} \end{aligned} \quad (14)$$

Here, we need to choose the value of  $h_1$  large enough so that most of the trajectories do not exist from  $\partial G_1$ . See the comments in Section 3.5.2.

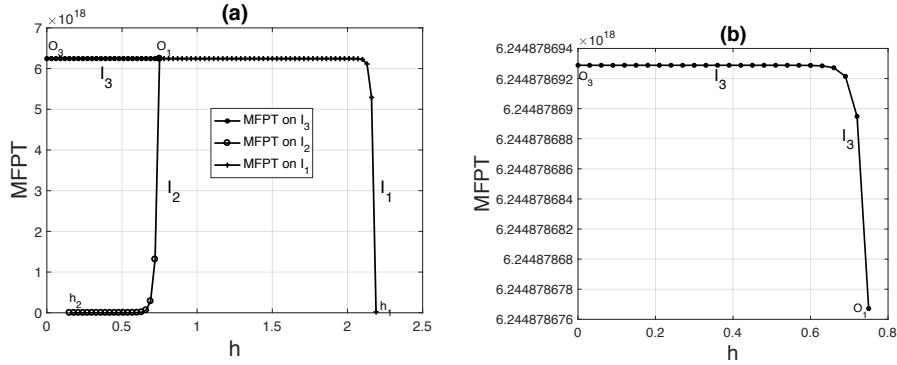


Figure 6: (a) The graph shows the MFPT from the bottom of the left well near  $O_3$  (at  $C_3(h_0)$ , with  $h_0$  slightly larger than 0), to first exit near the bottom of the right well at  $C_2(h_2)$ , with  $h_2 = 0.15$ , or first exit the region  $G$  above the saddle at  $C_1(h_1)$ , with  $h_1 = 2.2$ . (b) The graph is an enlargement of the first segment of Figure (6)(a).

## 3.5 Results and Comments

### 3.5.1 The Mesoscopic DNA is Robust Against Noise

Hence, the mean life span of collective base-flipping of the mesoscopic DNA,  $T_{DNA}$ , in the natural time should be

$$6.244878692881616 \times 10^{18} \times 0.9846 \text{ ps} = 6.1487 \times 10^{18} \text{ ps}$$

which is about 10 weeks. Since the life time of a skin cell is about 2 to 4 weeks, and  $T_{DNA} > T_{Cell}$ , we can reasonably conclude that it is robust against noise and will survive in a normal situation without radiation.

### 3.5.2 FW Theory is Essential in Studying Metastable Rate

Figure (6)(a) shows the MFPT from the bottom of the left well at  $C_3(h_0)$ , with  $h_0$  slightly larger than 0, to first exit near the bottom of the right well at

$C_2(h_2)$ , with  $h_2 = 0.15$ , or first exit the top of the region  $G$  at  $C_1(h_1)$ , with  $h_1 = 2.2$ . Figure (6)(b) is an enlargement of the first segment of Figure (6)(a). By studying the results encapsulated in Figure (6) closely, the diffusion process can be broadly divided into 3 consecutive segments:

1. in the first segment: it takes only less than  $10^{-6}$  % of the total MFPT ( $1.6163 \times 10^{10}$  unit of time) for the system to diffuse from the bottom of the left well to first exit the top of the left well at the level set  $C_3(h)$  with  $h = 0.75$ , which is the height of the well;
2. but in the second segment: it requires an extremely long time, namely, almost 80 % of the total MFPT ( $4.9329 \times 10^{18}$  unit of time) for the system to diffuse across the rank-one saddle, to first pass the top of the right well at the level set  $C_2(h)$  with  $h = 0.75$ , and to first exit the level set  $C_2(h)$  with  $h = 0.72$ , which indicates that the system has just slightly entered into the right well;
3. in the last segment: it takes another additional 20 % of the total MFPT for the process to finally first exit near the bottom of the right well at  $C_2(h)$  with  $h = 0.15$ .

From these observations, we would like to make a couple of remarks:

1. In studying the MFPT and metastable rate of a diffusion process, many papers use the standard Hamiltonian stochastic averaging method and restrict their attention to only one well. For a few DOF system, the results may be fine. But for a large DOF system, the results can be way off. We highly recommend others to use Freidlin-Wentzell method.
2. This method, in our opinion, can be readily extended to study the metastable rates and branching ratios, etc, of other multiple-well Langevin systems with weak noise, as long as the Hamiltonian is the only first integral and it satisfies some other general requirements, see the references [21, 22] for more details.

## 4 But It is Vulnerable to Specific THz Fields

After showing that the mesoscopic DNA is robust against noise, we would like to quantify the requirements for specific electric fields that can trigger its collective base-flipping dynamics and cause large amplitude separation of base pairs. Here, we will use the newly developed theory of resonant enhancement of the rate of metastable transition [9], which has built on the work of large deviation theory [22] and the results of researches in physics [16, 36, 15, 3, 33, 38].

Below, we will first briefly summarize the main result of this new theory of resonant enhancement and then apply it to our DNA model. We will find the requirements for the specific electric fields in the following steps: (1) we will obtain numerically the most probable path (MPP) which is essentially the

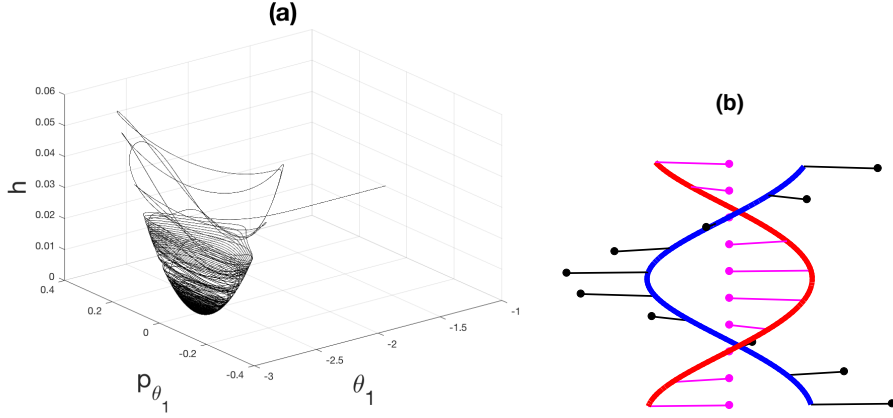


Figure 7: To apply the theory of resonant enhancement, we need to numerically compute the most probable path (MPP) which is essentially the heteroclinic connection between the metastable equilibrium point at the bottom of the left well and the rank-one saddle. See the text for more details. Figure (a) shows the 3D energy contour plot of the projection of the numerically computed  $2N$ -dimensional MPP onto the  $(\theta_1, p_{\theta_1})$  phase plane. The other similarly drawn 3D energy contour plots on the  $(\theta_n, p_{\theta_n})$  phase planes all share the similar feature. The MPP allows us to study the resonant enhancement of the base-flipping dynamics across the saddle whose configuration in the physical space is shown in Figure (b).

heteroclinic connection between the metastable equilibrium point at the bottom of the left well and the rank-one saddle; (2) we will derive analytically the formula for the work done by the electric field along the MPP that winds from the bottom to the top of the potential well; (3) we will use this formula to find, via numerical methods, the requirements for the specific electric fields and conclude that the mesoscopic DNA is vulnerable to THz fields with frequencies around 0.5 THz and with amplitudes in the order of 450 kV/cm. At the end of the section, (4) we will show that our semi-analytical results compare well with the experimental data of Titova et al. [41, 42, 43] which have demonstrated that they could affect the function of DNA in human skin tissues by THz pulses with frequencies around 0.5 THz and with a peak electric field at 220 kV/cm; (5) we will also briefly discuss the need to model the THz pulses and the need to have a better result on the issue of pre-factor.

#### 4.1 The Theory of Resonant Enhancement of Metastable Rate

For the convenience of readers, we will restate below the main result of Chao and Tao [9], namely, Theorem 2.7, in the similar notations as in the original paper.

**Theorem 2.7** Consider  $n$  particles in  $R^d$  whose equation of motion is given by the underdamped kinetic Langevin system perturbed by a periodic force  $f(x, t)$ :

$$\begin{aligned} dx &= v dt \\ dv &= -\Gamma v dt - \nabla V(x) dt + \epsilon f(x, t) dt + \sqrt{\mu} \Gamma^{\frac{1}{2}} dW \end{aligned} \quad (15)$$

Assume that

1.  $\mu < \epsilon$ ,
2.  $x_u$  is the only attractor on the separatrix between the basins of attraction of  $x_a$  and  $x_b$ , and the heteroclinic connection  $x_a$  to  $x_b$  exists in the noiseless ( $\mu = 0$ ) and forceless ( $\epsilon = 0$ ) system,
3.  $\epsilon$  is small enough such that a heteroclinic connection from  $x_a^\epsilon(t)$  to  $x_b^\epsilon(t)$  exists in the high order Euler-Lagrange equation.

Then the transition rate from  $x_a^\epsilon(t)$  to  $x_b^\epsilon(t)$  is asymptotically equivalent to  $\exp(-S^\epsilon/\mu)$ , i.e.,

$$\begin{aligned} R &\asymp e^{-\frac{S^\epsilon}{\mu}} \quad \text{where} \quad S^\epsilon = 2[V(x_u) - V(x_a)] + \epsilon \Delta S_e + O(\epsilon^2) \\ \Delta S_e &= \min_{t_0} \Delta S(t_0), \quad \Delta S(t_0) = -2 \int_{-\infty}^{+\infty} \dot{x}_h^T(t - t_0) f(x_h(t - t_0), t) dt \end{aligned} \quad (16)$$

and  $x_h(t)$  satisfies

$$\ddot{x}_h - \Gamma \dot{x}_h + \nabla V(x_h) = 0, \quad x_h(-\infty) = x_a, \quad x_h(+\infty) = x_u \quad (17)$$

## 4.2 Its Application to the New DNA Model

Recall here the non-dimensional equations of motion of our DNA model with noise and radiation

$$\begin{aligned} d\theta_n &= p_{\theta_n} dt \\ dp_{\theta_n} &= -\nu \kappa p_{\theta_n} dt - ((\theta_{n+1} - 2\theta_n + \theta_{n-1}) - \kappa U'(\theta_n)) dt \\ &\quad + \mathcal{E} (\kappa \sin(\theta_n + (n-1)\pi/5) \cos \Omega t) dt + \sqrt{2\beta^{-1}(\nu\kappa)}^{\frac{1}{2}} dW \end{aligned}$$

which are almost identical to the Equations (15), with

$$\begin{aligned} V(\theta) &= \sum_{n=1}^N \left[ \frac{1}{2} (\theta_n - \theta_{n-1})^2 + \kappa \left( e^{-a(1+\cos \theta_n - d_0)} - 1 \right)^2 \right] \\ f(\theta, t) &= \kappa \sin(\theta_n + (n-1)\pi/5) \cos \Omega t \end{aligned} \quad (18)$$

As stated earlier, the parameters are chosen to best represent the typical values for the opening and closing dynamics of DNA and are given by

1.  $\nu\kappa = 0.006564$  where  $\nu\kappa$  is the friction coefficient,
2.  $\kappa = \frac{D}{S} = 0.025$  where  $\kappa$  is the strength of the Morse potential,
3.  $\mu = 2\beta^{-1} = 2\frac{k_B T}{S} = 0.0267$  where  $2\beta^{-1}$  is the strength of the noise.

Moreover,  $\mathcal{E}$  is the moment of force (w.r.t the strength of Morse potential  $\kappa$ ) induced by the electric field in the non-dimensional system. The theory of resonant enhancement requires that  $\mathcal{E} > \mu$ , which means that  $\mathcal{E}$  needs to be larger than 0.0267.

Below, we will first, numerically, find the most probable path (MPP) which is essentially the heteroclinic connection between the metastable equilibrium point at the bottom of the left well and the rank-one saddle.

#### 4.2.1 Computation for the Most Probable Path–Heteroclinic Connection

As we have studied in Section 3, the DNA model has 2 stable equilibria  $W_L, W_R$  and a rank-one saddle  $S$  given by

$$\begin{aligned} W_L &= (-\theta_e, \dots, -\theta_e; 0, \dots, 0), & S &= (0, \dots, 0; 0, \dots, 0), \\ W_R &= (\theta_e, \dots, \theta_e; 0, \dots, 0), \end{aligned}$$

where  $\theta_e = \arccos(d_0 - 1) = 2.6906$ .

According to Theorem 2.7, we first need to find the most probable path, i.e, to approximate the heteroclinic connection from  $\theta_L$  to  $\theta_S$  of this noiseless and forceless system by numerically solving the uphill equations, Eqs. (17). However, since this is a second order boundary value problem with the boundary points at  $t = \pm\infty$ , it poses numerical difficulties. And the resonant enhancement theory [9] suggests to tackle them in the following steps:

1. First, reverse the time and solve the corresponding downhill equations from the saddle  $S$  to  $W_L$  with the sign flip on the velocity in the uphill equations.
2. Then, make the approximation by choosing an initial point as close as numerically feasible to the saddle, and in the unstable direction of the downhill vector field linearized at the saddle.
3. Finally, simulate this initial value problem using fourth-order Runge-Kutta for long enough time, with sufficiently small time steps, and collect the result backward in time.

Figure(7) shows the 3D energy contour plot of the projection of this  $2N$ -dimensional MPP onto the  $(\theta_1, p_{\theta_1})$  phase plane. The other similarly constructed 3D energy contour plots all share the similar feature.

### 4.2.2 Work Done Along the MPP and the Rate Enhancement

Next, we need to apply the general formula Eq. (16) to our DNA model. Following similar steps as in Chao and Tao [9], we can show that

$$\Delta S_e = -2 \left| \int_{-\infty}^{+\infty} \left[ \sum_{j=1}^N \kappa \dot{x}_h^j(t) \sin(x_h^j(t) + (j-1)\alpha) \right] e^{i\Omega t} dt \right| = -2\kappa |\mathcal{I}(\Omega)| \quad (19)$$

See Appendix B for details. Here, it is interesting to note that the integral term in Eq. (16), after rewritten as

$$\int_{-\infty}^{\infty} f^T(x_h(t-t_0), t) dx_h$$

can be seen as the work done, by the force  $f$ , along the MPP in the configuration space  $(x_h)$ , and in overcoming the potential difference of the well [37]

$$\delta V = [V(x_u) - V(x_a)].$$

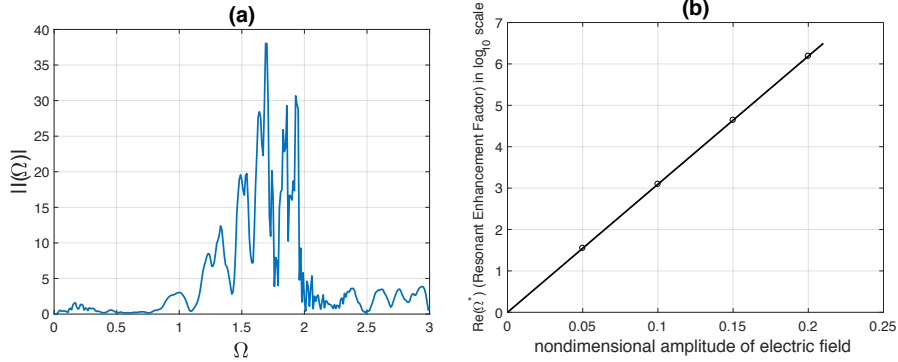


Figure 8: (a) The graph shows the relationship between  $|\mathcal{I}(\Omega)|$  and  $\Omega$ . We observe that there exists a special  $\Omega^* = 1.7$ , called resonant frequency, at which  $|\mathcal{I}(\Omega)|$  peaks. The graph has a broadband character between 1 to 3 (with peak at 1.7). This is due to the fact that (i) the system has 30 DOF with internal frequencies between 1.5 to 3, and (ii) it is a kinetic Langevin system with weak damping and noise. (b) The graph shows the relation between the resonant enhancement factor  $R_e(\Omega^*)$  and the non-dimensional amplitude of the electric field  $\mathcal{E}$ . For example, for  $\mathcal{E} = 0.1$ , we have  $R_e(\Omega^*) = 1.2411 \times 10^3$ ; and for  $\mathcal{E} = 0.2$ , we have  $R_e(\Omega^*) = 1.5404 \times 10^6$

Then the escape rate  $R$  from  $x_L^\mathcal{E}(t)$  to  $x_R^\mathcal{E}(t)$  is asymptotically equivalent to  $\exp(-S^\mathcal{E}/\mu)$  with  $\mu = 2\beta^{-1}$ , i.e.,

$$R \asymp e^{-\frac{S^\mathcal{E}}{\mu}}$$



where

$$\begin{aligned} S^\mathcal{E} &= 2\delta V + \mathcal{E}\Delta S_e + O(\mathcal{E}^2) \\ &= 2\delta V - 2\mathcal{E}\kappa|\mathcal{I}(\Omega)| + O(\mathcal{E}^2) \end{aligned}$$

It can be rewritten as

$$R = C(\mu) \times e^{-\frac{S^\mathcal{E}}{\mu}} = C(\mu) \times e^{-\frac{2\delta V}{\mu}} \times e^{\frac{2\mathcal{E}\kappa|\mathcal{I}(\Omega)|}{\mu}} \times e^{-\frac{O(\mathcal{E}^2)}{\mu}} \quad (20)$$

where the first exponent factor is related to the metastable rate of the forceless system, the second exponent factor  $R_e$  is related to the resonant enhancement due to the electric field with angular frequency  $\Omega$ , and the first factor  $C(\mu)$  is called prefactor whose appearance is due to fact that the result of Theorem 2.7 is only valid up to asymptotic equivalence<sup>5</sup>.

Now, with  $(x_h(t), \dot{x}_h(t)) = (\theta(t), p_\theta(t))$  of the heteroclinic orbit and the formula given by Eq. (19) in hand, we can study the dependence of  $\Delta S_e$  on the input frequency  $\Omega$  via  $\mathcal{I}(\Omega)$ . For each  $\Omega$ , we compute  $|\mathcal{I}(\Omega)|$  by numerically approximating the integral via piecewise trapezoidal quadrature with high enough resolution. Figure (8)(a) shows the relationship between  $|\mathcal{I}(\Omega)|$  and  $\Omega$ . We observe that there exists a special  $\Omega^* = 1.7$  at which  $|\mathcal{I}(\Omega)|$  peaks. In the theory of resonant enhancement, this frequency  $\Omega^*$  is called the resonant frequency. It is interesting to note here that the graph has a broadband character between 1 to 3 with peak at 1.7. This is due to the fact that (i) the system has 30 DOF with internal frequencies between 1.5 to 3, and (ii) it is a kinetic Langevin system with weak noise.

Moreover, if we call

$$R_e(\Omega) = e^{\frac{2\mathcal{E}\kappa|\mathcal{I}(\Omega)|}{\mu}} \quad (21)$$

loosely as the rate enhancement factor, then  $R_e(\Omega^*)$  at the resonant frequency  $\Omega^*$  can be seen as the resonant enhancement factor. Figure (8)(b) shows the relation between the resonant enhancement factor  $R_e(\Omega^*)$  and the non-dimensional amplitude of the electric field  $\mathcal{E}$  (w.r.t. the strength of the Morse potential). For example, for  $\mathcal{E} = 0.1$ , we have  $R_e(\Omega^*) = 1.2411 \times 10^3$ ; and for  $\mathcal{E} = 0.2$ , we have  $R_e(\Omega^*) = 1.5404 \times 10^6$

### 4.2.3 DNA is Vulnerable to THz Fields with High Amplitudes

With the resonant enhancement relationship encapsulated in Figure (8)(b) in hand, we are ready to find the requirements for specific electric fields that can trigger its collective base-flipping dynamics and cause large amplitude separation of base pairs.

1. First, we would like to recall our semi-analytical result on the mean first passage time (MFPT) of our forceless system. In Section 3, we have estimated that the life span of our mesoscopic DNA is given by

$$T_{DNA} \approx 6.2449 * 10^{18} \text{ ps} = 6.2449 \times 10^6 \text{ s}$$

<sup>5</sup>See Section 4.2.4 for further discussions

which is about 10 weeks. Correspondingly, its metastable rate is given by

$$R_0 \approx 1.601 \times 10^{-7}/\text{s}$$

Hence, for  $\mathcal{E}$  between 0.1 and 0.2, with its metastable rate enhancement factor between  $1.2411 \times 10^3$  and  $1.5404 \times 10^6$ , it seems reasonable to claim that electric fields with the resonant frequency  $\Omega^* = 1.7$  and with  $\mathcal{E}$  between 0.1 and 0.2 will induce collective base-flipping and cause large amplitude separation of base pairs <sup>6</sup>.

2. Before comparing the above results with the experimental data, we need to recall a couple of formulas from Section 2.2.2 that link  $\Omega$  and  $\mathcal{E}$  of the non-dimensional system to the frequency  $\nu_0$  and amplitude  $E$  of electric fields. According to the formula, Eq. (8), for  $\Omega^* = 1.7$ , the resonant frequency  $\nu_0^*$  of the required electric field is given by

$$\nu_0^* = 1.0156 \times (1.7/2\pi) = 0.1616 \times 1.7 \text{ THz} = 0.2748 \text{ THz}$$

which is a THz field that peaked at 0.2748 THz with a bandwidth 0.16-0.48 THz. This semi-analytical result is consistent with the experimental data of Titova et al. The broadband THz pulses in their experiments had an amplitude spectrum that peaked at 0.5 THz, with a bandwidth of 0.1-2.0 THz. <sup>7</sup>

3. According to the formula Eq. (7), for  $\mathcal{E}$  between 0.1 to 0.2, amplitudes of electric fields  $E$  are given by

$$E = 4.5033 \times 10^8 \times \mathcal{E} = 4.5033 \times \mathcal{E} \text{ (MV/cm)}$$

i.e., between 453.33 (kV/cm) and 906.66 (kV/cm). While these are indeed electric fields with high amplitude, they are also within the same order as the experimental data in Titova et al. whose peak electric field is equal to 220 kV/cm. <sup>8</sup>

In conclusion, we have shown that DNA is vulnerable to THz fields with high amplitudes and our semi-analytical result is consistent with the experimental data of Titova et al. In Section 4.3, we will elaborate further on the experimental setup of Titova et al. and discuss the issues of non-thermal effects, pulses vs waves, etc.

#### 4.2.4 The Need to Have a Better Result on the Issue of Prefactor

Recall that the proof in Chao and Tao [9] is based on the assumption that  $\mu < \epsilon$  so that it can first uses the large deviation principle and then the asymptotic

---

<sup>6</sup>See Section 4.2.4 for further discussions

<sup>7</sup>See Section 4.3 for more details.

<sup>8</sup>See Section 4.3 for more details.

analysis for the maximum likelihood path. Hence the result is in the form of asymptotic equivalence, i.e., the transition rate  $R$  is given by

$$R \asymp \exp((-2\delta V - \epsilon\Delta S_e + \mathcal{O}(\epsilon^2))/\mu)$$

which can be rewritten as

$$R = C(\mu) \times \exp(-2\delta V)/\mu \times \exp((- \epsilon\Delta S_e + \mathcal{O}(\epsilon^2))/\mu)$$

with  $C(\mu)$  as a pre-factor.

If  $\epsilon$  and  $\mu$  is not related, it looks tempting to let  $\epsilon \downarrow 0$  and one will have

$$R_0 = C(\mu) \times \exp(-2\delta V)/\mu$$

and then

$$R = R_0 \times \exp((- \epsilon\delta S_e + \mathcal{O}(\epsilon^2))/\mu)$$

This new formula, if true, will decompose the transition rate  $R$  into the product of two parts, the first part is the metastable rate of the forceless system, and the second part is the enhancement rate due to the forcing. Since the first part can be obtained via Freidlin-Wentzell theory of Hamiltonian Perturbations and the second part can be obtained via theory of metastable rate enhancement, we will be able to circumvent the issue of pre-factor.

However, since the proof in Chao and Tao [9] is based on  $\mu < \epsilon$ , the above reasonings need to be scrutinized carefully. And more work is needed to obtain a sharper result.

### 4.3 Comparison with Experiments of Titova et al.

In a series of papers [41, 42, 43], Titova et al. analyzed the effects of intense, broadband, picosecond-duration THz pulses on the DNA integrity in an artificial human skin tissue. Their work yielded an experimental demonstration of the disruptions of DNA function in an exposed skin tissue. Below, we will give a brief description of their experimental setup, and summarize two of their main findings that are relevant to our study, namely, (i) the effect is non-thermal, and (ii) the high peak electric field is likely responsible for the disruptions in DNA dynamics, or even DNA damage.

#### 4.3.1 The Experimental Setup of Titova et al.

The skin tissue was exposed to THz pulses with 1 kHz repetition rate. Each pulse had a pulse energy up to  $1 \mu\text{J}$ , and an amplitude spectrum that peaked at 0.5 THz with a bandwidth of 0.1-2.0 THz. The time of exposure was 10 minutes long. Duration of a THz pulse was 1.7 picosecond. Spot size of THz beam at the focus was 1.5 mm in diameter. Now, let  $W_{\text{THz}}$  be the pulse energy,  $\tau$  be the pulse duration,  $A$  be the area of beam focus with radius  $r$  equal to 0.75 mm, and  $Z_0 = 377$  ohm be the impedance of the free space. Titova et al. were able to use these experimental data and a couple of formulas to make their points.

### 4.3.2 The Effect was Non-Thermal in Their Experiments

As expected, by using picosecond duration THz pulse source with low repetition rates, the THz-pulse-induced heating effect was negligible. The exposure was carried out at 21° C and the time-averaged THz power density, which could be computed according to the following formula

$$(W_{THz}/A) \times 10^3/s = 57 \text{ mW/cm}^2,$$

was quite low. Applying the thermal model in Kristensen et al. [26], the estimated temperature increase at beam center due to THz exposure was less than 0.7° C. Moreover, none of the heat shock protein encoding genes were differentially expressed in the THz-exposed tissues. These allowed them to conclude that the biological effects of picosecond duration THz pulses were non-thermal as average power levels were insufficient to cause significant heating, and the levels of temperature-change-sensitive genes and proteins were unchanged.

### 4.3.3 The High Peak Electric Field Might Cause the Disruptions of DNA Dynamics

However, THz pulses with picosecond duration and 1  $\mu\text{J}$  energy have high instantaneous electric field which might cause disruptions in DNA dynamics and even DNA damage. For a THz pulse with Gaussian spatial profile, its peak electric field could be calculated from the pulse energy as follow:

$$E_{THz}^{\text{Peak}} = \sqrt{\frac{4Z_0W_{THz}}{\tau A}}$$

As it turned out, the peak electric field was 220 kV/cm which was extremely high. They concluded that these high peak electric fields were likely responsible for the observed THz-pulse-driven cellular effects.

Moreover, they mentioned in their papers the work of Alexandrov et al. in a favorable light and hoped to understand better the mechanism, and the specific requirements for the intensity and frequency of the radiation.

### 4.3.4 Our Work May Have Suggested the Mechanism and Provided the Requirements

As mentioned in the **Introduction**, by building on our earlier work [25], the insights from the controversy around the paper of Alexandrov et al., and especially the non-thermal experimental results of Titova et al., we develop a new mesoscopic DNA model. We start with the DNA in the fluid with thermal noise. But we disregard the additional thermal effects by ignoring radiation-fluid interactions, in order to focus our attention mainly on the effects of radiation on the DNA via coupling the electric field with the DNA bases. These new mesoscopic DNA model allows us to employ the Freidlin-Wentzell theory of stochastic averaging and the newly developed theory of resonant enhancement.

Our study has shown that while the mesoscopic DNA is metastable and robust to environmental effects, it is vulnerable to certain frequencies that could be targeted by specific THz fields for triggering its collective base-flipping dynamics and causing large amplitude separation of base pairs. Moreover, our semi-analytic estimates show that the required fields should be THz fields with frequencies around 0.28 THz and with amplitudes in the order of 450 kV/cm. These estimates compare well with the experiments of Titova et al., which have demonstrated that they could affect the function of DNA in human skin tissues by THz pulses with frequencies around 0.5 THz and with a peak electric field at 220 kV/cm.

We believe that our results may have suggested resonance as a possible mechanism for the experiments of Titova et al. and may have provided the specific requirements for the intensity and frequency of the radiation.

#### 4.3.5 The Need to Model THz Pulses

But of course more work is still needed to take into consideration the issue of modeling the pulses. In the experiments of Tiotva et. al., they skillfully used intense THz pulses with low repetition rates to obtain a sufficiently high peak electric field and to disrupt the DNA dynamics, or even cause DNA damage, in a non-thermal setting. In our present study, we try to theoretically investigate the mechanisms and requirements for such specific electric fields using the existing tools in the theory of control of stochastic mechanical systems. By ignoring the additional radiation-fluid interaction, we get ourselves into the non-thermal setting, minimize the impacts of the issue of waves vs pulses, and enable us to obtain some interesting and important results. And we wish that in the near future, further researches will be able to extend the present theory of resonant enhancement to the case where the driving radiation are pulses.

## 5 Conclusion and Future Work

Our new mesoscopic DNA model is a torsional model that takes into account not only the issues of helicity and the coupling of an electric field with the base dipole moments, but also includes environmental effects such as fluid viscosity and thermal noise. And all the parameter values are chosen to best represent the typical values for the opening and closing dynamics of a DNA. While it is different from the one used by Alexandrov et al., our semi-analytical results do suggest similar conclusion: DNA natural dynamic can be significantly affected by specific THz radiation exposure.

This new mesoscopic DNA model allows us to employ Freidlin-Wentzell theory of stochastic averaging and the newly developed theory of resonant enhancement. Our semi-analytic estimates show that the required fields should be THz fields with frequencies around 0.28 THz and with amplitudes in the order of 450 kV/cm. These estimates compare well with the experiments of Titova et al., which have demonstrated that they could affect the function of DNA in human

skin tissues by THz pulses with frequencies around 0.5 THz and with a peak electric field at 220 kV/cm. And we believe that our results may have suggested resonance as a possible mechanism for the experimental results of Titova et al. and may have provided the specific requirements for the intensity and frequency of the radiation.

But more work is needed to take into consideration the issue of modeling the pulses. And we wish that future research will extend the present theory of resonant enhancement to the case where the radiation are pulses, as suggested in Section 4.3.5. Besides, a better result on the issue of prefactor mentioned in Section 4.2.4 will also be important. As for the issue of inhomogeneity, our initial explorations and computations have convinced us that the frequencies and amplitudes of the required THz fields are definitely sequence dependent (A,T,G,C), but we will leave them to our next paper.

However, even as it stands right now, the new DNA model and the semi-analytical results may have already provided a better understanding of the resonant mechanism and hopefully will inspire new experimental designs that may settle this controversy. Moreover, we believe our semi-analytical methods may be useful in studying the metastable rate and its enhancement for chemical as well as other bio-molecular systems.

## Acknowledgments

We would like to dedicate this paper to the memory of Professor R. Stephen Berry for his generosity, helpful suggestions, and consistent encouragement. HO acknowledges support the Air Force Office of Scientific Research under MURI award number FA9550-20-1-0358 (Machine Learning and Physics-Based Modeling and Simulation). MT is partially supported by NSF DMS-1847802, NSF ECCS-1942523, Cullen-Peck Scholarship, and Emory-GT AI.Humanity Award.

## AUTHOR DECLARATIONS

### Conflict of Interest

The authors have no conflicts to disclose.

### Author Contributions

**W. S. Koon:** Conceptualization (equal); Formal analysis (lead); Methodology (lead); Software (equal); Writing-original draft (lead); Writing-review & editing (equal). **H. Owhadi:** Conceptualization (equal); Funding acquisition (equal); Methodology (supporting); Writing-review & editing (equal). **M. Tao:** Conceptualization (equal); Funding acquisition (equal); Methodology (supporting); Software (equal); Writing-review & editing (equal). **T. Yanao:** Conceptualization (equal); Methodology (supporting); Writing-review & editing (equal).

## DATA AVAILABILITY

The data that support the findings of this study are available from the corresponding author upon reasonable request.

## APPENDIX

### A FW Theory for Diffusion in Space with Multiple Wells

#### A.1 A Formula in Stochastic Averaging

Using the formula

$$\frac{d}{dh} \oint_{C(h)} G \cdot \frac{\nabla H}{|\nabla H|} dS = \oint_{C(h)} \nabla \cdot G \frac{dS}{|\nabla H|}$$

we can show that

$$\begin{aligned} \frac{d}{dh} u(h) &= \frac{d}{dh} \oint_{C(h)} (0, \nabla_p H) \cdot \frac{\nabla H}{|\nabla H|} dS \\ &= \oint_{C(h)} \nabla \cdot (0, \nabla_p H) \frac{dS}{|\nabla H|} = \oint_{C(h)} \Delta_p H \frac{dS}{|\nabla H|} = w(h) \end{aligned}$$

#### A.2 Computation of Drift and Diffusion Coefficients

Since the surface of  $C_i(h)$  can be represented as a  $(2N - 1)$ -dimensional graph in  $R^{2N}$ ,

$$p_1 = \pm \sqrt{2(h - V(q)) - \sum_{j=2}^N p_j^2}$$

surface integrals,  $u_i(h)$  and  $v_i(h)$ , can be transformed into volume integrals over the domains in the corresponding regions of the phase space

$$\Omega_i(h) = \left\{ (q, p_2, \dots, p_N) : \sum_{j=2}^N p_j^2 + 2V(q) \leq 2h \right\}$$

For  $v_i(h)$ , we have

$$v_i(h) = \oint_{C_i(h)} \frac{1}{|\nabla H|} dS = \int_{\Omega_i(h)} \frac{1}{|\nabla H|} \cdot \frac{|\nabla H|}{\nabla H \cdot \mathbf{e}_1} dq dp' = \int_{\Omega_i(h)} \frac{1}{p_1} dq dp'$$

where  $dp' = dp_2 \cdots dp_N$ . Similarly, for  $u_i(h)$  (and  $\alpha_i$ )

$$u_i(h) = \int_{\Omega_i(h)} \frac{\sum_{i=1}^N p_i^2}{p_1} dq dp'$$

For a few DOF systems, coefficients  $u_i(h), v_i(h)$  can be computed from these volume integral formulas using simply Monte Carlo method. But for a high DOF system like the DNA, we will reduce the dimension further by integrating  $dp'$  part analytically first and then employing more sophisticate MH Monte Carlo method to evaluate the remaining parts,  $A_i(h), B_i(h)$ , given below by

$$\begin{aligned} u_i(h) &= c \int_{\Sigma_i(h)} (h - V(q))^{\frac{N}{2}} dq = 2cA_i(h) \\ v_i(h) &= c \int_{\Sigma_i(h)} (h - V(q))^{\frac{N}{2}-1} dq = cB_i(h) \end{aligned}$$

where  $\Sigma_i(h) = \{q : V(q) \leq h\}$ . This is because

$$\begin{aligned} v_i(h) &= 2 \int_{\Sigma_i(h)} \int_{B(r(q))} \frac{1}{\sqrt{r(q)^2 - \sum_{j=2}^N p_j^2}} dp' dq \\ &= c \int_{\Sigma_i(h)} (h - U(q))^{\frac{N}{2}-1} dq \end{aligned}$$

where  $r(q) = \sqrt{2(h - V(q))}$  is the radius of the ball  $B(r(q))$ . Similar proof works for  $u_i(h)$ .

### A.3 Solutions for the 1D MFPT Equation on a Graph

- After first integration,

$$\frac{A_i(h)}{2} \frac{dM_i(h)}{dh} = e^{-\Psi_i(h)} \left[ \int_{h(O_k)}^{h(I_i)} -B_i(y) e^{\Psi_i(y)} dy + b_i \right]$$

For  $I_3$  at  $O_3$  (exterior), we have  $h(I_3) = h(O_3)$ . Since  $O_3$  is an exterior vertex,  $A_3(h(O_3)) = 0$ , we have

$$b_3 = 0$$

- At saddle  $O_1$ , the gluing condition allows us to equate the sum of the right hand side for  $I_3$  and  $I_2$  with those for  $I_1$ . After simplification, we obtain

$$\begin{aligned} b_1 &= e^{\Psi_3(h(O_1))} \left[ \int_{h(O_3)}^{h(O_1)} -B_3(y) e^{-\Psi_3(y)} dy \right] \\ &\quad + e^{\Psi_2(h(O_1))} \left[ \int_{h_2}^{h(O_1)} -B_2(y) e^{-\Psi_2(y)} dy + b_2 \right] \end{aligned}$$

- After further integrations, we impose the continuity condition for  $M(i, h)$  at the interior vertex  $O_1$ , and after simplifications, we obtain

$$c_1 = c_3 + \int_{h(O_3)}^{h(O_1)} \left[ \int_{h(O_3)}^z -B_3(y) e^{-\Psi_3(y)} dy \right] \frac{2e^{\Psi_3(z)}}{A_3(z)} dz$$



$$c_1 = c_2 + \int_{h_2}^{h(O_1)} \left[ \int_{h_2}^z -B_2(y) e^{-\Psi_2(y)} dy \right] \frac{2e^{\Psi_2(z)}}{A_2(z)} dz$$

$$+ b_2 \int_{h_2}^{h(O_1)} \frac{2e^{\Psi_2(z)}}{A_2(z)} dz$$

- The boundary condition at  $h_2$  gives us

$$c_2 = 0$$

- The boundary condition at  $h_1$  give us

$$0 = c_1 + \int_{h(O_1)}^{h_1} \left[ \int_{h(O_1)}^z -B_1(y) e^{-\Psi_1(y)} dy \right] \frac{2e^{\Psi_1(z)}}{A_1(z)} dz + b_1 \int_{h(O_1)}^{h_1} \frac{2e^{\Psi_1(z)}}{A_1(z)} dz$$

This system of six linear equations can be solved to provide the values for the parameters  $b_i$  and  $c_i$ . After evaluating all the relevant integrals  $[[B_i]]^{h(I_i)}$  and  $[A]^{h(I_i)}$ , we obtain

$$\begin{aligned} b_1 &= 18.831032678119339 \\ b_2 &= 0.418990478121480 \\ b_3 &= 0 \\ c_1 &= 1.094469943027227e + 15 \\ c_2 &= 0 \\ c_3 &= 1.094469945860001e + 15 \end{aligned}$$

## B Theory of Resonant Enhancement of Metastable Rate

Following similar steps as in [9], we show that

$$\Delta S_e = -2 \left| \int_{-\infty}^{+\infty} \left[ \sum_{j=1}^N \kappa \dot{x}_h^j(t) \sin(x_h^j(t) + (j-1)\alpha) \right] e^{i\Omega t} dt \right| = -2\kappa |\mathcal{I}(\Omega)|$$

This is because

$$\begin{aligned}
\Delta S(t_0) &= -2 \int_{-\infty}^{\infty} \left[ \sum_{j=1}^N \kappa \dot{x}_h^j(t) \sin(x_h^j(t) + (j-1)\alpha) \right] \cos(\Omega(t+t_0)) dt \\
&= -e^{i\Omega t_0} \int_{-\infty}^{\infty} \left[ \sum_{j=1}^N \kappa \dot{x}_h^j(t) \sin(x_h^j(t) + (j-1)\alpha) \right] e^{i\Omega t} dt \\
&\quad -e^{-i\Omega t_0} \int_{-\infty}^{\infty} \left[ \sum_{j=1}^N \kappa \dot{x}_h^j(t) \sin(x_h^j(t) + (j-1)\alpha) \right] e^{-i\Omega t} dt \\
&= -2 \cos(\Omega t_0) \mathcal{R}e \left( \int_{-\infty}^{\infty} \left[ \sum_{j=1}^N \kappa \dot{x}_h^j(t) \sin(x_h^j(t) + (j-1)\alpha) \right] e^{i\Omega t} dt \right) \\
&\quad + 2 \sin(\Omega t_0) \mathcal{I}m \left( \int_{-\infty}^{\infty} \left[ \sum_{j=1}^N \kappa \dot{x}_h^j(t) \sin(x_h^j(t) + (j-1)\alpha) \right] e^{i\Omega t} dt \right) \\
&= -2 \cos(\Omega t_0 + \phi) \left| \int_{-\infty}^{+\infty} \left[ \sum_{j=1}^N \kappa \dot{x}_h^j(t) \sin(x_h^j(t) + (j-1)\alpha) \right] e^{i\Omega t} dt \right|
\end{aligned}$$

where

$$\sin \phi = \frac{\mathcal{I}m \left( \int_{-\infty}^{\infty} \left[ \sum_{j=1}^N \kappa \dot{x}_h^j(t) \sin(x_h^j(t) + (j-1)\alpha) \right] e^{i\Omega t} dt \right)}{\left| \int_{-\infty}^{\infty} \left[ \sum_{j=1}^N \kappa \dot{x}_h^j(t) \sin(x_h^j(t) + (j-1)\alpha) \right] e^{i\Omega t} dt \right|}$$

Therefore,

$$\Delta S_e = \min_{t_0} \Delta S(t_0) = -2\kappa |\mathcal{I}(\Omega)|$$

## References

- [1] M. H. Abufadda, A. Erdelyi, E. Pollak, P. S. Nugraha, J. Hebling, J. A. Fulop, and L. Molnar, Terahertz pulses induce segment renewal via cell proliferation and differentiation overriding the endogenous regeneration program of the earthworm *Eisenia andrei*, *Biomed. Opt. Express* **2021**, 12, 1947-1961
- [2] B. S. Alexandrov, V. Gelev, A. R. Bishop, A. Usheva, and K.O. Rasmussen, DNA breathing dynamics in the presence of a terahertz field, *Phys. Lett. A* **374** (2010) 1214-1217
- [3] M. Assaf, A. Kamenev, and B. Meerson, Population extinction on a time-modulated environment, *Phys. Rev. E*, **78** (2008), 041123
- [4] K. J. Beers, Numerical Methods for Chemical Engineering, *Cambridge* 2007

- [5] N. Bou-Rabee and H. Owhadi, Long-run accuracy of variational integrations in the stochastic context, *SIAM J. NUMER. ANAL.* **48**, No. 1, 278-297
- [6] M. Bramanti, An Invitation to Hypocoelliptic Operators and Hormander's Vector Field, *Springer* 2014
- [7] M. Cadoni, R. De Leo, and Giuseppe, Composite model for DNA torsional dynamics, *Phys. Rev. E*, **75**, 021919 (2007)
- [8] G. Cai and W. Zhu, Elements of Stochastic Dynamics, *World Scientific* (2017)
- [9] Y. Chao and M. Tao, Parametric resonance for enhancing the rate of metastable transition, *SIAM J. APPL. MATH*, **82**, 3, 1068-1090
- [10] T. Dauxois, M. Peyard, and A. R. Bishop, Entropy-driven DNA denaturation, *Phys. Rev. E*, **47** (1993) R44
- [11] R. De Leo and S. Demelio, Numerical analysis of solitons profiles in a composite model for DNA torsion dynamics, *Int. J. of Non-Linear Mechanics*, **43** (2008) 1029-1039
- [12] M. Deng and W. Zhu, Energy diffusion controlled reaction rate in dissipative Hamiltonian systems, *Chinese Physics*, **16** No. 6 (2007)
- [13] M. Deng and W. Zhu, On the stochastic dynamics of molecular conformation, *J. Zhejiang Univ. Sci. A* (2007) 1401-1407
- [14] P. Du Toit, I. Mezic, and J. Marsden, Coupled oscillator models with no scale separation, *Physica D*, **238**, 490 (2009).
- [15] M. Dykman, B. Golding, L. Moccann, V. Smelyanskiy, D. Luchinsky, R. Mannella, and P. McClintock, Activated escape of periodically driven systems, *Chaos*, **11** (2001), 587-594
- [16] M. Dykman, H. Rabitz, V. Smelyanskiy, and H. Vugmeister, Resonant directed diffusion in nonadiabatically driven systems, *Phys. Rev. Lett.*, **79** (1997) 1178-1181
- [17] B. Eisenhower and I. Mezic, Targeted activation in deterministic and stochastic systems, *Phys. Rev. E*, **81**, 026603 (2010).
- [18] Englander S. W., Calhoun D. B., Englander J. J., Kallenbach N. R., Liem R. K., Malin E. L., Mandal C., Rogero J. R., Individual breathing reactions measured in hemoglobin by hydrogen exchange methods, *Biophys J.* 1980 Oct, **32**(1), 577-589.
- [19] M. I. Freidlin, Random and deterministic perturbations of nonlinear oscillators, *Doc. Math. J.. DMV* (1998) 223-235

- [20] M. I. Freidlin and M. Weber, Random perturbations of nonlinear oscillators, *Ann. Probab.*, **26**, No. 3 (1998) 925-967
- [21] M. I. Freidlin and M. Weber, On random perturbations of hamiltonian systems with many degrees of freedom, *Stochastic Processes and their Applications*, **94**, (2001) 199-239
- [22] M. I. Freidlin and A. D. Wentzell, Random Perturbations of Dynamical Systems, *Springer*, 2012
- [23] Gabern, F., W. S. Koon, J. E. Marsden, and S. D. Ross [2005], Theory and computation of non-RRKM lifetime distributions and rates in chemical systems with three or more degrees of freedom, *Physica D* **211**, 391–406.
- [24] C. M. Hough, D. N. Purschke, C. Huang, L. V. Titova, O. V. Kovalchuk, B. J. Warkentin, and F. A. Hegmann, Intense terahertz pulses inhibit Ras signaling and other cancer-associated signaling pathways in human skin tissue models, *J. Phys.,: Photonics* **2021**, 3, 034004
- [25] W. S. Koon, H. Owhadi, M. Tao, and T. Yanao, Control of a model of DNA division via parametric resonance, *Chaos*, **23** 01317 (2013)
- [26] T. Kristensen, W. Withayachumnankul, and P. Uhd Jeosen, and D. Abbott, Modeling terahertz heating effects on water, *Optics Express* **18**, No. 5 (2010)
- [27] B. Leimkuhler and C. Matthews, Molecular Dynamics, with Deterministic and Stochastic Numerical Methods, *Springer* 2015
- [28] A. G. Markelz and D. M. Mittleman, Perspective on terahertz applications in bioscience and biotechnology, *ACS Photonics* **2022**, 9, 1117-1126
- [29] I. Mezic, On the dynamics of molecular conformation, *Proc. Natl. Acad. Sci*, **103** (20) (2006) 7542-7547.
- [30] H. C. Ottinger, Stochastic Processes in Polymeric Fluids. Tools and Examples for Developing Simulation Algorithms, *Springer* 1996
- [31] G. A. Pavliotis, Stochastic Processes and Applications, Diffusion Processes, the Fokker-Planck and Langevin Equations, *Springer* 2014
- [32] M. Peyard and A. R. Bishop, Statistical mechanics of a nonlinear model for DNA denaturation, *Phys. Rev. Lett.*, **62** (1989) 2755\*
- [33] F. Riahi, On Lagrangians with high order derivatives, *Ann. J. Phys.*, **40** (1972), 386-390
- [34] D. M. Sitnikov, I. V. Ilina, V. A. Revkova, A. Rodionov, S. A. Gurova, R. O. Shatalova, A. V. Kovalev, A. V. Ovchinnikov, O. V. Chefonov, M. A. Konoplyannikov, V. A. Kalsin, and V. P. Baklaushev, Effects of hight intensity non-ionizing terahertz radiation on human skin fibroblasts, *Biomed. Opt. Express* **2021**, 12, 7122-7138

- [35] I. Sizov, M. Rahman, B. Gelmont, M. Norton, and T. Globus, Sub-THz spectroscopic characterization of vibrational modes in artificially designed DNA monocrystal, *Chemical Physics* 425 (2013) 121-125
- [36] V. Smelyanskiy, M. Dykman, H. Rabitz, and H. Vugmeister, Fluctuation, escape, and nucleation in driven systems, *Phys. Rev. Lett.*, **79** (1997) 3113-3116
- [37] V. Smelyanskiy, P. McClintock, R. Mannella, D. Luchinsky, and M. Dykman, Thermally activated escape of driven systems: the activation energy *J. Phys. A Math. Gen.*, **32** (1999)
- [38] A. Souza and M. Tao, Metastable transition in inertial Langevin systems: what can be different from the overdamped case? *European J. Appl. Math.*, **30** (2019) 830-852
- [39] D. W. Stroock and S. R. S. Varadhan, Multidimensional Diffusion Processes, *Springer* 1997
- [40] E. S. Swanson, Modeling DNA response to terahertz radiation, *Phys. Rev. E* **83** (2011)
- [41] L. V. Titova, A. K. Ayesheshim, A. Golubov, D. Fogen, R. Rodriguez-Juarez, R. Woycicki, F. A. Hegmann, and O. Kovalchuk, Intense THz pulses cause H2AX phosphorylation and activate DNA damage response in human skin tissue, *Biomed. Opt. Express* **4** (2013)
- [42] L. V. Titova, A. K. Ayesheshim, A. Golubov, R. Rodriguez-Juarez, A. Kovalchuk, F. A. Hegmann, and O. Kovalchuk, Intense picosecond THz pulses alter gene expression in human skin tissue in vivo, *Proc. of SPIE*, **8585** (2013)
- [43] L. V. Titova, A. K. Ayesheshim, A. Golubov, R. Rodriguez-Juarez, R. Woycicki, F. A. Hegmann, and O. Kovalchuk, Intense THz pulses down-regulate genes associated with skin cancer and psoriasis: a new therapeutic avenue? *Sci. Rep.* 2013, **3**, 2363
- [44] L. Yakushevich, *Nonlinear Physics of DNA*, Wiley-VCH, 2004.
- [45] S. Yomosa, Soliton excitations in deoxyribonucleic acid (DNA) double helices, *Phys. Rev. A*, **27**, Number 4 (1983)
- [46] C.-T. Zhang, Harmonic and subharmonic resonances of microwave absorption in DNA, *Phys. Rev. A* **40**, 2148-2153 (1989).